Journal of Nuclear Medicine, published on April 19, 2018 as doi:10.2967/jnumed.118.208611

Anti-MISRII radiolabeled antibodies: new tools for a theranostic approach in ovarian cancer

Emmanuel Deshayes[1,2*], Riad Ladjohounlou[1*], Pierre Le Fur[1], Alexandre Pichard[1], Catherine Lozza[1], Vincent Boudousq[1], Samuel Sevestre[1], Marta Jarlier[2], Roxana Kashani[3], Joanna Koch[3], Jane Sosabowski[3], Julie Foster[3], Nicolas Chouin[4], Frank Bruchertseifer[5], Alfred Morgenstern[5], Pierre-Olivier Kotzki[2], Isabelle Navarro-Teulon[1⁂] and Jean-Pierre Pouget[1⁂]

[1] IRCM, Institut de Recherche en Cancérologie de Montpellier, INSERM U1194, Université de Montpellier, Institut régional du Cancer de Montpellier, Montpellier, F-34298, France; [2] Institut régional du Cancer de Montpellier, Montpellier, F-34298, France; [3] Centre for Molecular Oncology, Barts Cancer Institute, Queen Mary University of London, UK; [4] ONIRIS, Nantes, France; [5]Directorate for Nuclear Safety and Security, European Commission - Joint Research Centre, Karlsruhe, Germany.

*These authors contributed equally to this work

⁂ Co-last authors

Corresponding author: Jean-Pierre Pouget, PhD, INSERM U1194, Institut de Recherche en Cancérologie, 34298 Montpellier cedex 5, Tel. 33 467 613 708
E-mail: jean-pierre.pouget@inserm.fr

Running title: Anti-MISRII radiolabeled antibody

Key words: targeted radiotherapy, radioimmunotherapy, theranostic, MISRII, ^{213}Bi, ^{177}Lu, ovarian, peritoneal carcinomatosis

Abstract

We have developed the 16F12 mouse monoclonal antibody (mAb) that targets the MISRII receptor expressed by ovarian tumors. Here, we assessed in preclinical models the possibility to use radiolabeled 16F12 in a theranostic approach for small-volume ovarian peritoneal carcinomatosis, for instance after cytoreductive surgery.

Methods: DOTA-, DTPA- or DFO-conjugated 16F12 mAb was radiolabeled with beta (^{177}Lu) or alpha (^{213}Bi) particle emitters for therapeutic use, and with ^{89}Zr for positron emission tomography (PET) imaging. At day 13 post-xenograft, mice bearing intraperitoneal MISRII-positive AN3CA endometrial carcinoma cell tumor xenografts were treated by conventional intraperitoneal radioimmunotherapy (IP-RIT) with 10 MBq ^{177}Lu-16F12 or 12.9 MBq ^{213}Bi-16F12, or by brief intraperitoneal radioimmunotherapy (BIP-RIT) using 50 MBq ^{177}Lu-16F12 or 37 MBq ^{213}Bi-16F12. For BIP-RIT, 30 minutes after injection of radiolabeled mAbs, the peritoneal cavity was washed to remove the unbound radioactivity. The biodistribution of ^{177}Lu- and ^{213}Bi-16F12 mAbs was determined and then used for dose assessment. Hematological toxicity was also monitored.

Results: The 16F12 mAb was satisfactorily radiolabeled for both therapy and imaging. IP-RIT with ^{177}Lu-16F12 was slightly more efficient in delaying tumor growth than IP-RIT with ^{213}Bi-16F12. Conversely, ^{213}Bi-16F12 was more efficient than ^{177}Lu-16F12 in BIP-RIT. The biodistribution analysis showed that the tumor-to-blood uptake ratio was significantly higher with BIP-RIT than with IP-RIT for both ^{213}Bi- and ^{177}Lu-16F12. Hematological toxicity was more pronounced with ^{177}Lu-16F12 than ^{213}Bi-16F12. SPECT/CT (after BIP-RIT with ^{177}Lu-16F12) and PET/CT images (after injection of ^{89}Zr-16F12 in the tail vein) showed focal uptake at the tumor site.

Conclusion: Radiolabeled 16F12 could represent a new theranostic tool for small volume ovarian peritoneal carcinomatosis. Specifically, ^{213}Bi-16F12-based BIP-RIT could be proposed to selected

patients as an alternative adjuvant treatment immediately after cytoreductive surgery. An anti-MISRII mAb is currently being used in a First in Human study, thus making radiolabeled anti-MISRII mAbs a realistic theranostic option for the clinic.

Introduction

Ovarian cancer (OC) is the most lethal gynecologic malignancy (*1*). Most OCs (90%) are of epithelial origin (EOC), while sex cord/stromal (including granulosa cell tumors, GCTs) and germ cell tumors account for the remaining 10%. Optimal treatment is usually based on cytoreductive surgery to remove the macroscopic disease and on systemic chemotherapy with paclitaxel and carboplatin. However, the 5-year overall survival rate remains poor (46%) (*2*), partly because, in most patients, OC is a "silent killer" that progresses without detectable symptoms or clinical signs. This leads to late-stage diagnosis (over 70% at stage III or IV), when the disease has spread to the peritoneal cavity as peritoneal carcinomatosis (PC). PC treatment relies on cytoreductive surgery to remove the macroscopic disease followed by intraperitoneal (IP) adjuvant platinum-based chemotherapy with significant increase in overall survival and progression-free survival compared with intravenous chemotherapy (*3*). Although many women respond well to this therapeutic approach, disease recurs in 70 to 90% of responders, but remains localized in the peritoneal cavity. In the 1960s, Sugarbaker proposed the combination of cytoreductive surgery and hyperthermic IP chemotherapy (HIPEC) to treat the residual disease in selected patients with PC (*4*). HIPEC increases survival of patients with primary recurrent disease and it is today used as first-line or second-line therapy (*5*). However, as morbidity has been one of the main drawbacks of HIPEC, it is not recommended outside of clinical trials (*6*).

Many studies have investigated the efficacy of radioimmunotherapy (RIT) as a therapeutic option for PC using beta (*7-17*), alpha (*18-23*) (*24*) or Auger particle (*25-27*) emitters in preclinical and clinical models (*28*). Particularly, RIT at the surgery block could represent an advantage over the current treatments. In 2010, we proposed brief intraperitoneal radioimmunotherapy (BIP-RIT) (*25*) for the treatment of colorectal cancer PC in mice. BIP-RIT includes the IP injection of high

activities of radiolabeled monoclonal antibodies (mAbs) that are left in the peritoneal cavity for less than 1 hour, as is the case for HIPEC. Then, the peritoneal cavity is extensively washed with saline solution using a peristaltic pump to remove the unbound radioactivity (Figure 1).

To specifically target OC, we developed the 16F12 murine mAb against the human Müllerian Inhibiting Substance type II receptor (MISRII; also known as Anti-Müllerian hormone type II receptor). The ligand for MISRII is anti-Müllerian hormone (AMH), a 140 kDa dimeric glycoprotein, also called Müllerian inhibiting substance (MIS). MIS is a member of the transforming growth factor-β family that regulates tissue growth and differentiation (*29*). Human MISRII is a 66 kDa glycosylated single transmembrane domain receptor that includes a 17 amino acid (aa) signal peptide, a 127aa extracellular region, a 26aa transmembrane domain and an intracellular region of 403aa bearing the serine/threonine kinase activity (*30,31*). MISRII is detected in 100% of GCTs (*32*) and in almost 70% of EOC, in 77% of ovarian dysgerminomas and 75% of endometrial cancers (*33*), as well as in ascites cells isolated from patients with OC (*34,35*). Thus, MISRII is highly expressed in many different gynecologic cancers, including tumors that lack effective systemic therapies.

In this preclinical study, we compared the therapeutic efficacy and hematological toxicity of the 16F12 mAb radiolabeled with beta (^{177}Lu) or alpha (^{213}Bi) particle emitters administered by conventional IP-RIT and by BIP-RIT. We also assessed ^{89}Zr-16F12 for positron emission tomography (PET) imaging.

Materials and Methods

Cell line and antibodies

The AN3CA human endometrial carcinoma cell line was from the American Type Culture Collection (ATCC, Manassas, VA, USA). AN3CA cells were cultured in MEM medium with 10% fetal calf serum, 1% penicillin, 0.1% streptomycin, 1% sodium pyruvate and 1% non-essential amino acids. MISRII expression in AN3CA cells was confirmed by flow cytometry analysis when the cells were received and again before each xenograft. The anti-MISRII 16F12 mAb was isolated from mouse hybridoma ascites, as previously described (*36*).

Animals

Female athymic nude-Foxn1^{nu} mice (6–8 week-old) (Envigo RMS Laboratories, Gannat, France) were kept in the animal facility for at least one week before use. They were housed at 22°C and 55% humidity, light-dark cycle of 12h, and ad libitum food and water. Body weight was monitored weekly and mice were examined throughout the study. They were IP or subcutaneously xenografted with 4.5×10^6 AN3CA cells in RPMI medium with Matrigel (ratio 1:1) in a volume of 200µL. All animal experiments were performed in compliance with the French government guidelines and the INSERM standards for experimental animal studies (agreement B34-172-27). They were approved by the ethics committees of the Institut de Recherche en Cancérologie de Montpellier (IRCM/INSERM) and the Languedoc Roussillon region (CEEA LR France No. 36) for animal experiments (reference number: 1056).

Conjugation of the 16F12 mAb with DOTA, DTPA or DFO

16F12-DOTA

Prior to radiolabeling with ^{177}Lu, 16F12 was conjugated with *p*-SCN-Bn-DOTA. Briefly, *p*-SCN-Bn-DOTA (Macrocyclics, Dallas, TX, USA) was dissolved in conjugation buffer (0.05M $NaHCO_3$-Na_2CO_3, 0.15M NaCl, 5mM EDTA, pH 8.8) diluted (1/10) before use. Next, 16F12 was

added at 15 fold molar excess and incubated with stirring at 25°C for 19h. To remove free chelator, the mixture was washed 3 times with conjugation buffer using Amicon ultra-15 centrifugal filter units (Merck-Millipore, St Quentin en Yvelines, France), and then 3 times with 5mM ammonium acetate buffer (pH 7.0). The average number of DOTA molecules per mAb was assessed as previously described (*37*) and was between 5 and 7. All steps were performed in metal-free conditions.

16F12-DTPA

Before radiolabeling with ^{213}Bi, 16F12 was conjugated with 2-(*p*-SCN-benzyl)-cyclohexyl acid A-diethylenetriaminepentaacetic (SCN-CHX-A"-DTPA, Macrocyclics, Dallas, TX, USA). A solution of 0.35 mg of SCN-CHX-A"-DTPA dissolved in 1 ml of conjugation buffer (0.05M $NaHCO_3$-Na_2CO_3, 0.15M NaCl pH 8.5-8.9 containing 0.01M EDTA pH 4.5) was diluted (1/10) and mixed with 5mg of 16F12 at 15 fold molar excess. The mixture was stirred at 25°C overnight. To remove unconjugated SCN-CHX-A"-DTPA, the mixture was washed using Amicon ultra-15 centrifugal filter units 3 times with conjugation buffer, and then three times with 1 mL of 0.15M NaCl/0.05M sodium acetate (pH 7.2). The number of chelates/mAb was determined using the Pb(II)-Arsenazo III method (*37*) and was generally between 5 and 7. All steps were performed in metal-free conditions.

16F12-DFO

The protocol described by Vosjan *et al.* was followed and slightly modified (*38*). Between 2 and 10 mg 16F12 mAb (13.2–66 nmol) dissolved in 1 mL buffer (0.1 M sodium carbonate,) at pH 9.0 was incubated with 20µL (2–10 mM) p-isothiocyanatobenzyl-desferrioxamine B (Df–Bz–NCS, Macrocyclics, Dallas, TX, USA) dissolved in DMSO and incubated for 30 min at 37°C using a thermomixer at 550 rpm. The reaction mixture was purified on a PD-10 size exclusion column (GE

Healthcare, Buckinghamshire, UK) equilibrated on (and eluted with) 5 $mg.ml^{-1}$ gentisic acid in 0.25 M sodium acetate (pH 5.4–5.6).

Radiolabeling of conjugated 16F12

Production of ^{177}Lu-DOTA-16F12 (further called ^{177}Lu-16F12)

For radiolabeling, 3.7 mg DOTA-16F12 was incubated with 740MBq $^{177}LuCl_3$ (Perkin Elmer, Boston, Ma, USA) at 37°C in 0.25M sodium acetate (pH 5.5) for 45min. The reaction was quenched with 100 µL of 1mM DTPA. Radiolabeled mAbs were separated from free ^{177}Lu through a PD-10 column equilibrated with 10mg/mL PBS-HSA. The specific activity was between 150 and 250MBq/mg ^{177}Lu-DOTA-16F12.

Production of ^{213}Bi-DTPA-16F12 (further called ^{213}Bi-16F12)

^{213}Bi was eluted from the ^{225}Ac generator provided by the Institute for Transuranium Elements (Karlsruhe, Germany) using a mixture of 0.3 ml of 0.2M HCl and 0.3 mL of 0.2M NaI. The eluate was collected directly into 0.12 ml of 4M sodium acetate and 0.05 ml of 20% ascorbic acid. The mixture (pH 5.3-5.5) was incubated with DTPA-16F12 (37 MBq/mg) at room temperature (RT) for 5min. The reaction was quenched with 10 µL of 1.5mg/ml DTPA.

Production of ^{89}Zr-DFO-16F12 (further called ^{89}Zr-16F12)

The radiolabelling of Df-Bz-NCS-16F12 was performed as follows: 50 – 61 MBq ^{89}Zr oxalate, 31-33 µL of 1M HEPES and 26-28 µL of 2M NaOH were combined with 200-500 µg of mAb and the reaction mixture was incubated for 1.5 h at room temperature. Reactions were then purified using a NAP5 column equilibrated on 0.25 M sodium acetate and fractions were collected. Fractions of purity greater than 99% (iTLC-SG, Varian, 20 mM citrate, pH 5.5) were combined and used for administration to animals (100 – 120 MBq/mg). Immunoreactive fraction of the purified product using the Lindmo assay in ANC3A cells was shown to be 1 (*39*).

Radiochemical purity and immunoreactivity

Immediately after radiolabeling, ^{177}Lu-16F12 and ^{213}Bi-16F12 mAbs were purified through PD-10 columns equilibrated with 10 mg/mL PBS-HSA. The radiochemical purity was determined using iTLC paper (iTLC-SG, Varian) with 0.05M sodium citrate pH 5.5, as mobile phase. The conjugated mAb immunoreactivity was checked using a Gallios Flow Cytometer (Beckman Coulter, Brea, CA).

IP-RIT and BIP-RIT

At day 13 after tumor cell xenograft when tumor size was about 80-100 mm^3, mice were divided into six groups (n=7). Two groups were treated by IP-RIT with 500µL of either ^{177}Lu-16F12 (200MBq/mg, 10MBq) or ^{213}Bi-16F12 (37MBq/mg, 12.95MBq). Two groups were treated by BIP-RIT, where 30 minutes after IP injection of high activities (500µL of either ^{177}Lu-16F12 mAb (200MBq/mg, 50MBq) or ^{213}Bi-16F12 mAb (37MBq/mg, 37MBq)), the peritoneal cavity was washed with 20 mL of saline solution (Figure 1A). Previous experiments showed that a single injection of non-radiolabeled 16F12 at the concentration used for IP-RIT or BIP-RIT is not accompanied by therapeutic efficacy (data not shown). Control groups included mice that received NaCl according to the IP-RIT and BIP-RIT methods.

The mouse weights were recorded throughout the study and no clinical signs of pain or distress were seen. Mice were sacrificed at different time points (10, 20 and 30 days post-RIT) to measure the tumor mass (i.e., sum of the weight of all tumor nodules).

Biodistribution analysis after IP-RIT or BIP-RIT

For the biodistribution studies, radiolabelled antibody doses were supplemented with unlabeled 16F12 to administer similar amounts of antibodies as during treatment. Thirteen days post-xenograft, mice (n=4/group) received an IP injection of 500µL ^{177}Lu-16F12 (40MBq/mg, 2MBq) or ^{213}Bi-16F12 (16.8MBq/mg, 5.9MBq) (IP-RIT), or of 500 µl ^{177}Lu-16F12 (40MBq/mg, 10MBq)

or ^{213}Bi-16F12 (10.2MBq/mg, 10.2MBq) followed by peritoneal cavity wash as described previously (BIP-RIT).

Mice were sacrificed at 3, 24, 48, 72 and 168h after injection of ^{177}Lu-16F12, and at 1, 2 and 3h after injection of ^{213}Bi-16F12. Blood and healthy organs were collected, weighed and radioactivity was measured using a gamma-well counter (Hewlett Packard, Palo Alto, CA). Due to the small tumor size, the tumor mass was determined by measuring the tumor volume using ImageJ® and by assuming a tumor density of 1.05 g.cm^{-3}. The total tumor mass per mouse was calculated as the sum of the mass of all tumor nodules.

For IP-RIT, the percentage of injected activity per gram of tissue (%IA/g), corrected for the radioactive decay, was calculated. For BIP-RIT, because of the peritoneal cavity wash, the percentage of the residual activity per gram of tissue (%RA/g) corrected for the radioactive decay was determined. This required measuring the total activity in the whole body at the time of dissection.

Dosimetric studies

Biodistribution data were used to evaluate the radioactivity uptake per tissue mass (Bq/g) as a function of time. Time-activity curves (TAC) for each organ and tumors were fitted by a mono-exponential decay function or the sum of two exponential functions using the PRISM 7 software (GraphPad Software, Inc., San Diego, CA). The Akaike Information Criterion was used to select the best fitting function (*40*). In general, the sum of two exponential functions was used for IP-RIT with ^{177}Lu (except for tumors and muscle for which the mono-exponential decay was preferred), whereas for BIP-RIT with ^{177}Lu and ^{213}Bi and for IP-RIT with ^{213}Bi, a mono-exponential decay fitting curve was chosen (with the exception of muscle for BIP-RIT with ^{213}Bi). The time-integrated activity for each organ and tumors was derived by calculating the area under the curve of each fitted TAC. The absorbed dose was then calculated using the MIRD formalism (*41*). The TAC for

bone marrow was calculated based on the blood data, considering a red marrow to blood activity ratio of 0.4, because 16F12 is a full IgG that is not known to bind specifically to bone marrow (*42*). For ^{213}Bi experiments, absorbed doses were calculated assuming a local energy deposition within all organs and tumors: time-integrated activities, weighed by the tissue mass, were multiplied by the energy of the emitted alpha particles (8.32 MeV per decay, considering the contribution of ^{213}Bi and ^{213}Po with the appropriate branching ratio, according to the MIRD radionuclide data and decay schemes (*43*)). For ^{177}Lu experiments, cross-fire irradiation between organs could contribute significantly to the absorbed doses received by the different organs. Therefore, the S-values calculated for ^{177}Lu in a previously described 22g-mouse model (*44*) were used. Self-dose S-values were scaled to the measured organ masses. For bone marrow, the calculation was performed only for femoral bone marrow. Finally, self-dose S-values for tumors were calculated using the Monte Carlo code GATE (*45*). Tumors were modeled using a unit density sphere with a 1.1 mm radius.

Hematological toxicity

Hematological toxicity was assessed in tumor-free athymic nude mice after IP-RIT or BIP-RIT with ^{213}Bi-16F12 and ^{177}Lu-16F12. After RIT, 12 µL of blood was collected from the tail in vials coated with EDTA, twice a week for 3 weeks and then every week. White blood cell (WBC) number and hemoglobin levels were quantified using the scil Vet abc system (SCIL Animal Care Co., Altfort, France).

SPECT and PET imaging using 16F12

^{177}Lu emits short-range beta particles and also low energy gamma particles that are suitable for gamma imaging. Therefore, whole-body SPECT/CT images were acquired at different time points (24, 48, 72 and 96h post-RIT), using a four-headed NanoSPECT imager (Bioscan Inc., Washington DC, USA). The system was equipped with a tungsten-based collimator with nine 1mm-diameter pinholes. The energy window was centered at 210keV with ±20% width. Acquisition times were

defined to obtain 30 000 counts for each projection (generally 60-120 seconds were required) with 24 projections. The total scan time was 30-60 minutes. Micro-CT whole-body images were acquired simultaneously (55kV, 500 milliseconds, 240 projections). Reconstructed data from SPECT and CT images were visualized and co-registered using Invivoscope® (Invicro, Inc., Washington, USA). Images and maximum intensity projections (MIPs) were reconstructed using the dedicated Invivoscope® software.

For PET imaging, one 7-week-old female Foxn1^{nu} mouse with a subcutaneous tumor xenograft in the left flank received 8 MBq of ^{89}Zr-DFO-16F12 via i.v. injection, and PET imaging was performed under 1.5% isoflurane/oxygen (1 L/min) anesthesia at 24, 48, 72 and 96h post-injection. Images were acquired using an Inveon PET/CT scanner (Siemens Preclinical Solutions Knoxville, TN, USA) and the following CT parameters: 80 kV tube voltage, 500 µA tube current, 400ms exposure time. Then, PET images were acquired using a 350-650 keV energy window and reconstructed to a 128x128x159 matrix with a voxel size of 0.776x0.776x0.796 mm using the 3D ordered-subset expectation maximization (OSEM3D) reconstruction algorithm with CT attenuation and scatter correction (two OSEM3D iterations, 18 MAP iterations).

Statistical analysis

Data were described using means (standard deviation) and medians (range). Treatment groups were compared using the non-parametric Kruskal-Wallis test. All statistical tests were bilateral, and the statistical significance level was set at 5%. Statistical analyses were done using the STATA 13.0 software (Stata Corporation, College Station, TX, USA).

Results

Therapeutic efficacy of BIP-RIT and IP-RIT

First, the mean total activity was monitored at different times after BIP-RIT and IP-RIT in mice bearing IP AN3CA cell tumor xenografts. For BIP-RIT with ^{177}Lu-16F12, the whole body activity dropped from 50MBq to 3.8MBq (7.6% of the injected activity) immediately after washing of the peritoneal cavity (Figure 1B). This value was quite close to the activity measured after IP-RIT (3.4MBq). However, SPECT/CT images (Figure 1C) showed that ^{177}Lu-16F12 was concentrated in tumors after BIP-RIT, whereas it diffused also into healthy tissues after IP-RIT.

In the NaCl-treated groups (control), tumors reached a mass of 1g in all mice by day 20 post-treatment (Figure 2). IP-RIT with 10 MBq ^{177}Lu-16F12 strongly reduced tumor growth, as indicated by the significantly smaller tumor mass compared with controls already at day 10 (1.3± 1×10^{-3}g vs 6± 4×10^{-2} g) (p=0.017) (Figure 2A).

In mice treated by BIP-RIT with 50MBq ^{177}Lu-16F12, tumor mass tended to be smaller than in controls at day 10. However, tumors progressively grew and by day 30 they were all bigger than 1g (Figure 2B). In mice treated by IP-RIT with 12.95 MBq ^{213}Bi-16F12, tumor growth was strongly reduced (p=0.0102), with a mean tumor mass of 3.3± 0.9×10^{-2}g at day 30 (>1g in controls) (Figure 2C). This effect was even more marked (p=0.0047) after BIP-RIT with 37 MBq ^{213}Bi-16F12 (mean tumor size of 1.2×10^{-2}± 8×10^{-3}g at day 30) (Figure 2D). Overall, BIP-RIT with ^{213}Bi-16F12 was more efficient in delaying tumor growth than IP-RIT with ^{213}Bi-16F12 (p=0.0339).

After BIP-RIT, radiolabeled 16F12 concentrates mainly in tumors

Biodistribution analysis (corrected for decay) indicated that the maximal tumor uptake of ^{177}Lu-16F12 was 8.9±3.1 %IA/g at 3h after IP-RIT and the maximal blood uptake (at 24h) was 15.9±1.04 %IA/g (Figure 3A). After BIP-RIT, the maximal tumor (at 3h) and blood uptake (at 24h) of ^{177}Lu-16F12 were 18.3±6.8 %RA/g and 14.3±11.9 %RA/g, respectively (Figure 3B).

For ^{213}Bi-16F12, biodistribution analysis (corrected for decay) showed that the maximal tumor (at 1h) and blood (at 3h) uptake were 3.0±1.7%IA/g and 5.0±1.2%IA/g, respectively, after IP-RIT

(Figure 3C), and 90.2±19.3%RA/g (at 1h) and 15.05±8.1 %RA/g (at 2h), respectively, after BIP-RIT (Figure 3D).

Incorporated activity and absorbed doses

For IP-RIT with ^{177}Lu-16F12 (Figure 4A), the activity concentration in blood (not corrected for decay) increased between 3 and 24h post-RIT and then progressively decreased. For BIP-RIT, the activity concentration in blood was much lower and decreased after 3 hours. Conversely, the tumor TACs (Figure 4B) were comparable for both RIT modalities with ^{177}Lu-16F12 (i.e., the activity concentration decreased after 3h), but the activity concentration was much higher for IP-RIT than BIP-RIT. For IP-RIT and BIP-RIT with ^{213}Bi-16F12, TACs for blood (Figure 4C) and for tumors (Figure 4D) could be fitted with a mono-exponential function. For BIP-RIT, the blood activity concentration was much lower than for IP-RIT whereas the activity concentrations within the tumors were of similar magnitude for BIP-RIT and IP-RIT.

At therapeutic activities, absorbed dose calculations for ^{177}Lu-16F12 or ^{213}Bi-16F12 after IP-RIT or BIP-RIT in tumors, blood, liver and kidneys (Figures 5 and 6; Tables 1 and 2) showed that they were always higher in healthy tissues after IP-RIT than BIP-RIT, irrespective of the radioimmunoconjugate used. In tumors, the ^{177}Lu-16F12 absorbed dose was higher with IP-RIT than for BIP-RIT, whereas that of ^{213}Bi-16F12 was higher with BIP-RIT. The mean absorbed dose (Tables 1 and 2) in tumors was then 5.6 (±2.1) Gy after IP-RIT with 10MBq of ^{177}Lu-16F12, and 2.5 Gy (±1) after BIP-RIT with 50MBq of ^{177}Lu-16F12. Conversely, it was higher after BIP-RIT with 37 MBq ^{213}Bi-16F12 than after IP-RIT with 12.95MBq ^{213}Bi-16F12) (3 Gy ±2.98 versus 2.2Gy ±2.9). Moreover, the absorbed doses in healthy organs were higher after IP-RIT than BIP-RIT with ^{177}Lu-16F12 and also, to a lesser extent, with ^{213}Bi-16F12 (Tables 1 and 2).

Hematological toxicity and weight loss

Hematological toxicity was assessed by quantifying WBC number and hemoglobin level. Compared with controls (NaCl), WBC number was significantly reduced by 70% at day 10 after IP-RIT with ^{177}Lu-16F12, but values were back to normal within 30 days. Conversely, WBC number was not negatively affected after BIP-RIT with ^{177}Lu-16F12 or after BIP-RIT and IP-RIT with ^{213}Bi-16F12 (Figure 7A). IP-RIT with ^{177}Lu-16F12 also transiently affected hemoglobin values (decrease by 30% compared with control at day 10) (Figure 7B), and led to significant weight loss. Conversely, weight continued to increase in the other three RIT groups (Figure 7C).

PET imaging

PET/CT images acquired at different time points after injection in the tail vein of ^{89}Zr-16F12 showed focal uptake at the site of the subcutaneous AN3CA cell tumor xenograft (Figure 7B).

Discussion

In this study we assessed whether the new murine 16F12 mAb against human MISRII can be used as a theranostic tool in small volume ovarian peritoneal carcinomatosis. For therapy, the 16F12 mAb was radiolabeled with ^{177}Lu or with ^{213}Bi and two routes of administration were compared: conventional IP-RIT and the BIP-RIT developed by our team (*25*). BIP-RIT feasibility immediately after cytoreductive surgery, considering both radiation protection and technical constraints, has already been validated at the Montpellier Cancer Institute.

As shown by SPECT/CT imaging and biodistribution/dosimetry studies, the main advantage of BIP-RIT compared with IP-RIT is the higher tumor-to-blood uptake ratio. For example, using the mean absorbed dose values from Tables 1 and 2, the tumor-to-blood absorbed dose ratios for the ^{213}Bi-16F12 mAb are 1.4 and 6 after IP-RIT and BIP-RIT, respectively. This confirms our previous results obtained with an anti-CEA mAb radiolabeled with ^{125}I (*25*). Moreover, we found that the

tumor-to-blood absorbed dose ratio was higher with ^{213}Bi than with ^{177}Lu (0.4 and 0.6 for IP-RIT and BIP-RIT with ^{177}Lu-16F12). This can be explained by the fact that the ^{213}Bi short physical half-life corresponds roughly to the incubation time of the radioactive solution in the peritoneal cavity - due to removal of unbound radioactivity, decays occur mainly in the peritoneal cavity before systemic diffusion of the antibody in other healthy organs.

In terms of efficacy, IP-RIT was slightly more efficient with ^{177}Lu-16F12 than with ^{213}Bi-16F12 (mean tumor mass: 0.01±0.003g and 0.03±0.01 g, respectively, at day 30; p=0.0339). The mean tumor absorbed doses calculated for ^{177}Lu and ^{213}Bi were 5.6 and 2.2 Gy, in agreement with the observed therapeutic effect. At day 30, an approximate relative biological effectiveness (RBE) of 2.5 (i.e., 5.6/2.2) could be calculated by assuming that tumor masses were quite similar (relative to the control tumour size limit of 1g). This RBE value is slightly lower than that reported in the literature (between 4 and 5) (*46,47*). The difference could be explained by the uncertainties associated with RBE calculations in this case (in particular, only one biological endpoint considered). Also strict RBE calculations refers to low LET 225kV X-rays and not to beta particles. Although ^{177}Lu-16F12 was the most efficient after IP-RIT, hematological toxicity was much lower with ^{213}Bi-16F12, in agreement with the mean absorbed doses for ^{177}Lu-16F12 and ^{213}Bi-16F12 in blood (13.5 and 1.6 Gy) and bone marrow (4.6 and 0.65 Gy) after IP-RIT. BIP-RIT with ^{177}Lu-16F12 did not have any therapeutic effect on tumor growth. Conversely, BIP-RIT with ^{213}Bi-16F12 efficiently reduced tumor growth (mean tumor mass of 0.012 ± 0.008 g at day 30). This difference could be partly explained by the mean tumor absorbed doses: 2.5 Gy for ^{177}Lu-16F12 and 3 Gy for ^{213}Bi-16F12. No hematological toxicity was observed after BIP-RIT using 50MBq ^{177}Lu-16F12, possibly due to the lower transfer of radioactivity from the peritoneal cavity to blood (less than 10% in 30min) during BIP-RIT compared with IP-RIT (activity in blood 30min post-

injection/injected activity ratio around 3). This suggests that the ^{177}Lu-16F12 injected activity could be increased to improve the therapeutic efficacy.

The advantage of using BIP-RIT with ^{213}Bi-mAbs is clear because this modality is associated with higher therapeutic efficacy and lower mean absorbed doses in healthy tissues compared with IP-RIT. Typically, BIP-RIT allowed decreasing the blood absorbed dose from 4.3 to 0.5 Gy, which could be a crucial advantage in the case of therapeutic combinations with chemotherapeutic drugs.

Conclusion

Our findings indicate that BIP-RIT with ^{213}Bi-16F12 could be an attractive solution for adjuvant RIT at the surgery block immediately after cytoreduction to eliminate the residual microscopic disease. Like for HIPEC, this approach should be proposed to selected patients. Moreover, a first in human study using the anti-MISRII GM102 mAb in ovarian cancers is currently ongoing (NCT02978755). Compared with unlabeled antibodies, a radiolabeled anti-MISRII mAb could provide a diagnostic (when labeled with ^{89}Zr) and therapeutic (labeled with ^{177}Lu or ^{213}Bi) advantage. Specifically, the radiolabeled antibodies can kill, through cross-fire irradiation and bystander effects (unpublished data), tumor cells that cannot be directly reached by the naked antibody. It is likely that the use of ^{177}Lu-16F12 would be most advantageous when administered systemically to patients already treated by BIP-RIT.

Disclosure

This research was funded by the French National Research Agency under the program ‘‘Investissements d’avenir’’ Grant agreement LabEx MAbImprove: ANR-10- LABX-53, Electricité de France Comité de Radioprotection (**RB 2017-12)**, Ligue Nationale Contre le Cancer (RF16011FF-RAB160).

Acknowledgments

The authors are grateful to Dr. Erik Larsson (Lund University, Sweden), who provided the S-values for lutetium-177 absorbed dose calculations.

References

1. Ferlay J, Soerjomataram I, Dikshit R, et al. Cancer incidence and mortality worldwide: sources, methods and major patterns in GLOBOCAN 2012. *Int J Cancer.* 2015;136:E359-386.

2. Siegel RL, Miller KD, Jemal A. Cancer statistics, 2016. *CA Cancer J Clin.* 2016;66:7-30.

3. Jaaback K, Johnson N, Lawrie TA. Intraperitoneal chemotherapy for the initial management of primary epithelial ovarian cancer. *Cochrane Database Syst Rev.* 2016:CD005340.

4. Bhatt A, Glehen O. The role of Cytoreductive Surgery and Hyperthermic Intraperitoneal Chemotherapy (HIPEC) in Ovarian Cancer: A Review. *Indian J Surg Oncol.* 2016;7:188-197.

5. Huo YR, Richards A, Liauw W, Morris DL. Hyperthermic intraperitoneal chemotherapy (HIPEC) and cytoreductive surgery (CRS) in ovarian cancer: A systematic review and meta-analysis. *Eur J Surg Oncol.* 2015;41:1578-1589.

6. Goodman MD, McPartland S, Detelich D, Saif MW. Chemotherapy for intraperitoneal use: a review of hyperthermic intraperitoneal chemotherapy and early post-operative intraperitoneal chemotherapy. *J Gastrointest Oncol.* 2016;7:45-57.

7. Muller C, Zhernosekov K, Koster U, et al. A unique matched quadruplet of terbium radioisotopes for PET and SPECT and for alpha- and beta- radionuclide therapy: an in vivo proof-of-concept study with a new receptor-targeted folate derivative. *J Nucl Med.* 2012;53:1951-1959.

8. Liu XY, Su X, Xie CJ, Li L, Yan JY, Sun ZY. Pharmacodynamic study of 131I-labeled CA215 antibody on an animal model of estrogen-resistant OC-3-VGH ovarian cancer. *Exp Ther Med.* 2015;10:572-578.

9. Grunberg J, Lindenblatt D, Dorrer H, et al. Anti-L1CAM radioimmunotherapy is more effective with the radiolanthanide terbium-161 compared to lutetium-177 in an ovarian cancer model. *Eur J Nucl Med Mol Imaging.* 2014;41:1907-1915.

10. Fischer E, Grunberg J, Cohrs S, et al. L1-CAM-targeted antibody therapy and (177)Lu-radioimmunotherapy of disseminated ovarian cancer. *Int J Cancer.* 2012;130:2715-2721.

11. Seidl C, Zockler C, Beck R, Quintanilla-Martinez L, Bruchertseifer F, Senekowitsch-Schmidtke R. 177Lu-immunotherapy of experimental peritoneal carcinomatosis shows comparable effectiveness to 213Bi-immunotherapy, but causes toxicity not observed with 213Bi. *Eur J Nucl Med Mol Imaging.* 2011;38:312-322.

12. Milenic DE, Wong KJ, Baidoo KE, et al. Targeting HER2: a report on the in vitro and in vivo pre-clinical data supporting trastuzumab as a radioimmunoconjugate for clinical trials. *MAbs.* 2010;2:550-564.

13. Zacchetti A, Coliva A, Luison E, et al. (177)Lu- labeled MOv18 as compared to (131)I- or (90)Y-labeled MOv18 has the better therapeutic effect in eradication of alpha folate receptor-expressing tumor xenografts. *Nucl Med Biol.* 2009;36:759-770.

14. Syme A, McQuarrie S, Fallone BG. Beta dose-rate distributions in microscopic spherical tumors for intraperitoneal radioimmunotherapy. *International Journal of Radiation Oncology*Biology*Physics.* 2003;56:1495-1506.

15. Borchardt PE, Quadri SM, Freedman RS, Vriesendorp HM. Indium-111- and yttrium-90-labeled human monoclonal immunoglobulin M targeting of human ovarian cancer in mice. *J Nucl Med.* 1998;39:476-484.

16. Borchardt PE, Quadri SM, Freedman RS, Vriesendorp HM. Intraperitoneal radioimmunotherapy with human monoclonal IGM in nude mice with peritoneal carcinomatosis. *Cancer biotherapy & radiopharmaceuticals.* 2000;15:53-64.

17. Janssen ML, Pels W, Massuger LF, et al. Intraperitoneal radioimmunotherapy in an ovarian carcinoma mouse model: effect of the radionuclide. *International Journal of Gynecological Cancer.* 2003;13:607-613.

18. Elgqvist J, Andersson H, Back T, et al. Alpha-radioimmunotherapy of intraperitoneally growing OVCAR-3 tumors of variable dimensions: Outcome related to measured tumor size and mean absorbed dose. *J Nucl Med.* 2006;47:1342-1350.

19. Gustafsson AM, Back T, Elgqvist J, et al. Comparison of therapeutic efficacy and biodistribution of 213Bi- and 211At-labeled monoclonal antibody MX35 in an ovarian cancer model. *Nucl Med Biol.* 2012;39:15-22.

20. Andersson H, Elgqvist J, Horvath G, et al. Astatine-211-labeled antibodies for treatment of disseminated ovarian cancer: an overview of results in an ovarian tumor model. *Clin Cancer Res.* 2003;9:3914S-3921S.

21. Palm S, Back TA, Lindegren S, Hultborn R, Jacobsson L, Albertsson P. Model of intraperitoneal targeted alpha-particle therapy shows post-therapy cold antibody boost (PT-CAB) enhances microtumor radiation dose and treatable tumor sizes. *J Nucl Med.* 2017.

22. Gustafsson-Lutz A, Back T, Aneheim E, et al. Therapeutic efficacy of alpha-radioimmunotherapy with different activity levels of the (213)Bi-labeled monoclonal antibody MX35 in an ovarian cancer model. *EJNMMI Res.* 2017;7:38.

23. Back T, Chouin N, Lindegren S, et al. Cure of Human Ovarian Carcinoma Solid Xenografts by Fractionated alpha-Radioimmunotherapy with (211)At-MX35-F(ab')2: Influence of Absorbed Tumor Dose and Effect on Long-Term Survival. *J Nucl Med.* 2017;58:598-604.

24. Boudousq V, Bobyk L, Busson M, et al. Comparison between internalizing anti-HER2 mAbs and non-internalizing anti-CEA mAbs in alpha-radioimmunotherapy of small volume peritoneal carcinomatosis using 212Pb. *PLoS One.* 2013;8:e69613.

25. Boudousq V, Ricaud S, Garambois V, et al. Brief intraperitoneal radioimmunotherapy of small peritoneal carcinomatosis using high activities of noninternalizing 125I-labeled monoclonal antibodies. *J Nucl Med.* 2010;51:1748-1755.

26. Santoro L, Boutaleb S, Garambois V, et al. Noninternalizing monoclonal antibodies are suitable candidates for 125I radioimmunotherapy of small-volume peritoneal carcinomatosis. *J Nucl Med.* 2009;50:2033-2041.

27. Baranowska-Kortylewicz J. Intraperitoneal radioimmunotherapy: Auger electron emitters for solid tumors. *Immunotherapy.* 2011;3:491-494.

28. Verheijen RH, Massuger LF, Benigno BB, et al. Phase III trial of intraperitoneal therapy with yttrium-90-labeled HMFG1 murine monoclonal antibody in patients with epithelial ovarian cancer after a surgically defined complete remission. *J Clin Oncol.* 2006;24:571-578.

29. Teixeira J, Maheswaran S, Donahoe PK. Mullerian inhibiting substance: an instructive developmental hormone with diagnostic and possible therapeutic applications. *Endocr Rev.* 2001;22:657-674.

30. Imbeaud S, Faure E, Lamarre I, et al. Insensitivity to anti-mullerian hormone due to a mutation in the human anti-mullerian hormone receptor. *Nat Genet.* 1995;11:382-388.

31. Jamin SP, Arango NA, Mishina Y, Hanks MC, Behringer RR. Genetic studies of the AMH/MIS signaling pathway for Mullerian duct regression. *Mol Cell Endocrinol.* 2003;211:15-19.

32. Rey R, Sabourin JC, Venara M, et al. Anti-Mullerian hormone is a specific marker of sertoli- and granulosa-cell origin in gonadal tumors. *Hum Pathol.* 2000;31:1202-1208.

33. Bakkum-Gamez JN, Aletti G, Lewis KA, et al. Mullerian inhibiting substance type II receptor (MISIIR): a novel, tissue-specific target expressed by gynecologic cancers. *Gynecol Oncol.* 2008;108:141-148.

34. Song JY, Chen KY, Kim SY, et al. The expression of Mullerian inhibiting substance/anti-Mullerian hormone type II receptor protein and mRNA in benign, borderline and malignant ovarian neoplasia. *Int J Oncol.* 2009;34:1583-1591.

35. Pepin D, Sosulski A, Zhang L, et al. AAV9 delivering a modified human Mullerian inhibiting substance as a gene therapy in patient-derived xenografts of ovarian cancer. *Proc Natl Acad Sci U S A.* 2015;112:E4418-4427.

36. Salhi I, Cambon-Roques S, Lamarre I, et al. The anti-Mullerian hormone type II receptor: insights into the binding domains recognized by a monoclonal antibody and the natural ligand. *Biochem J.* 2004;379:785-793.

37. Dadachova E, Chappell LL, Brechbiel MW. Spectrophotometric method for determination of bifunctional macrocyclic ligands in macrocyclic ligand-protein conjugates. *Nucl Med Biol.* 1999;26:977-982.

38. Vosjan MJ, Perk LR, Visser GW, et al. Conjugation and radiolabeling of monoclonal antibodies with zirconium-89 for PET imaging using the bifunctional chelate p-isothiocyanatobenzyl-desferrioxamine. *Nat Protoc.* 2010;5:739-743.

39. Lindmo T, Boven E, Cuttitta F, Fedorko J, Bunn PA, Jr. Determination of the immunoreactive fraction of radiolabeled monoclonal antibodies by linear extrapolation to binding at infinite antigen excess. *J Immunol Methods.* 1984;72:77-89.

40. Kletting P, Kull T, Reske SN, Glatting G. Comparing time activity curves using the Akaike information criterion. *Phys Med Biol.* 2009;54:N501-507.

41. Loevinger R, Budinger T, Watson E. *MIRD Primer for Absorbed Dose Calculations*. New York: Society of Nuclear Medicine; 1991.

42. Behr TM, Sgouros G, Stabin MG, et al. Studies on the red marrow dosimetry in radioimmunotherapy: an experimental investigation of factors influencing the radiation-induced myelotoxicity in therapy with beta-, Auger/conversion electron-, or alpha-emitters. *Clin Cancer Res.* 1999;5:3031s-3043s.

43. Eckerman KF, Akira E. *MIRD: Radionuclide Data and Decay Schemes*: by Society for Nuclear Medicine; 2008.

44. Larsson E, Ljungberg M, Strand SE, Jonsson BA. Monte Carlo calculations of absorbed doses in tumours using a modified MOBY mouse phantom for pre-clinical dosimetry studies. *Acta Oncol.* 2011;50:973-980.

45. Sarrut D, Bardies M, Boussion N, et al. A review of the use and potential of the GATE Monte Carlo simulation code for radiation therapy and dosimetry applications. *Med Phys.* 2014;41:064301.

46. Dahle J, Abbas N, Bruland OS, Larsen RH. Toxicity and relative biological effectiveness of alpha emitting radioimmunoconjugates. *Curr Radiopharm.* 2011;4:321-328.

47. Graf F, Fahrer J, Maus S, et al. DNA Double Strand Breaks as Predictor of Efficacy of the Alpha-Particle Emitter Ac-225 and the Electron Emitter Lu-177 for Somatostatin Receptor Targeted Radiotherapy *pLOS oNE.* 2014;9:e88239.

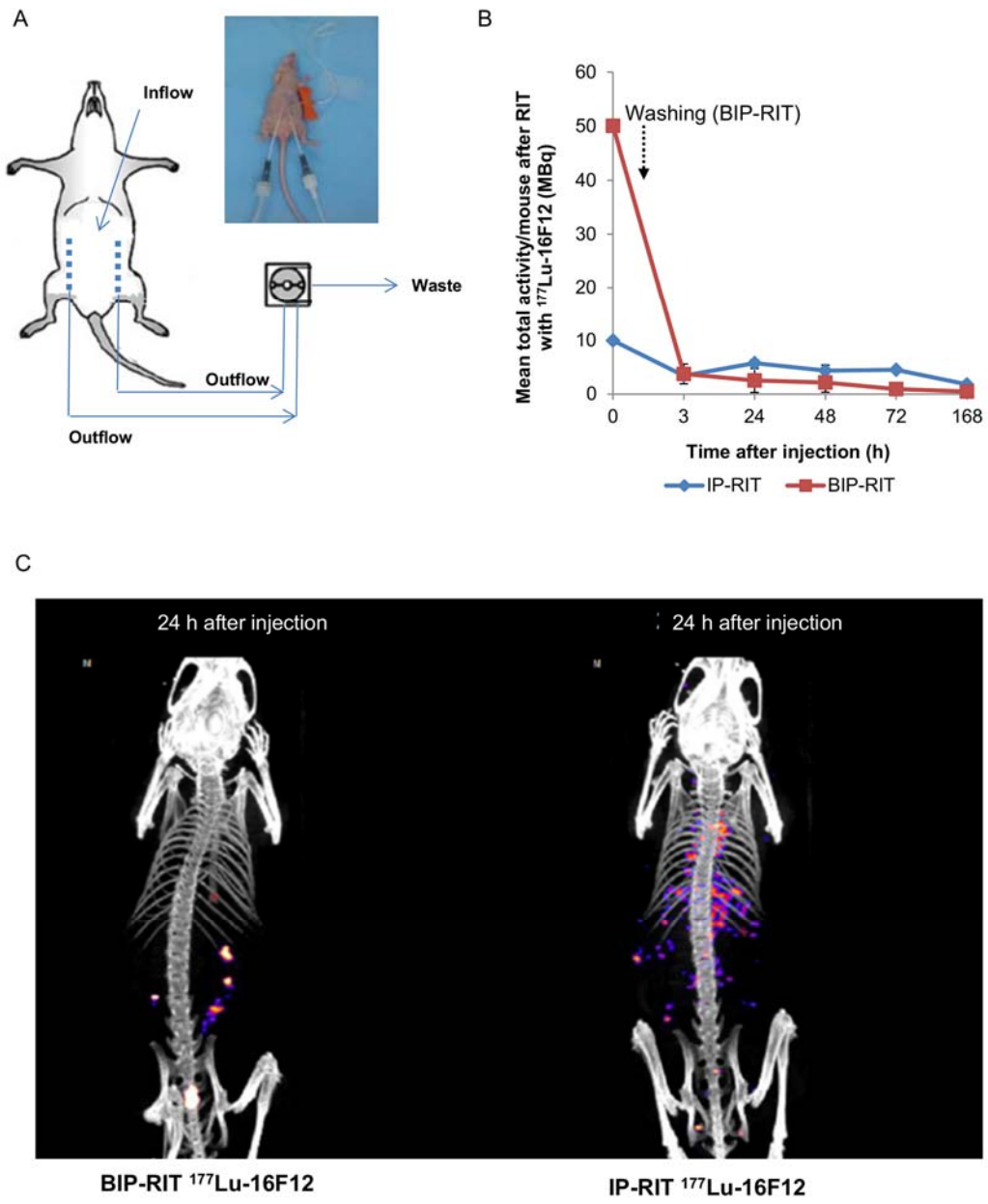

FIGURE 1. Schematic representation of the BIP-RIT approach (A). Mean activity per whole mouse body at different time points after BIP-RIT (red line, 50MBq) and IP-RIT (blue line, 10MBq) with ^{177}Lu-16F12 (n=7 mice/group) (B). Merged whole body SPECT/CT images of mice bearing AN3CA endometrial carcinoma cell tumor xenografts at 24h after BIP-RIT (red arrows show tumor nodules) or IP-RIT (C).

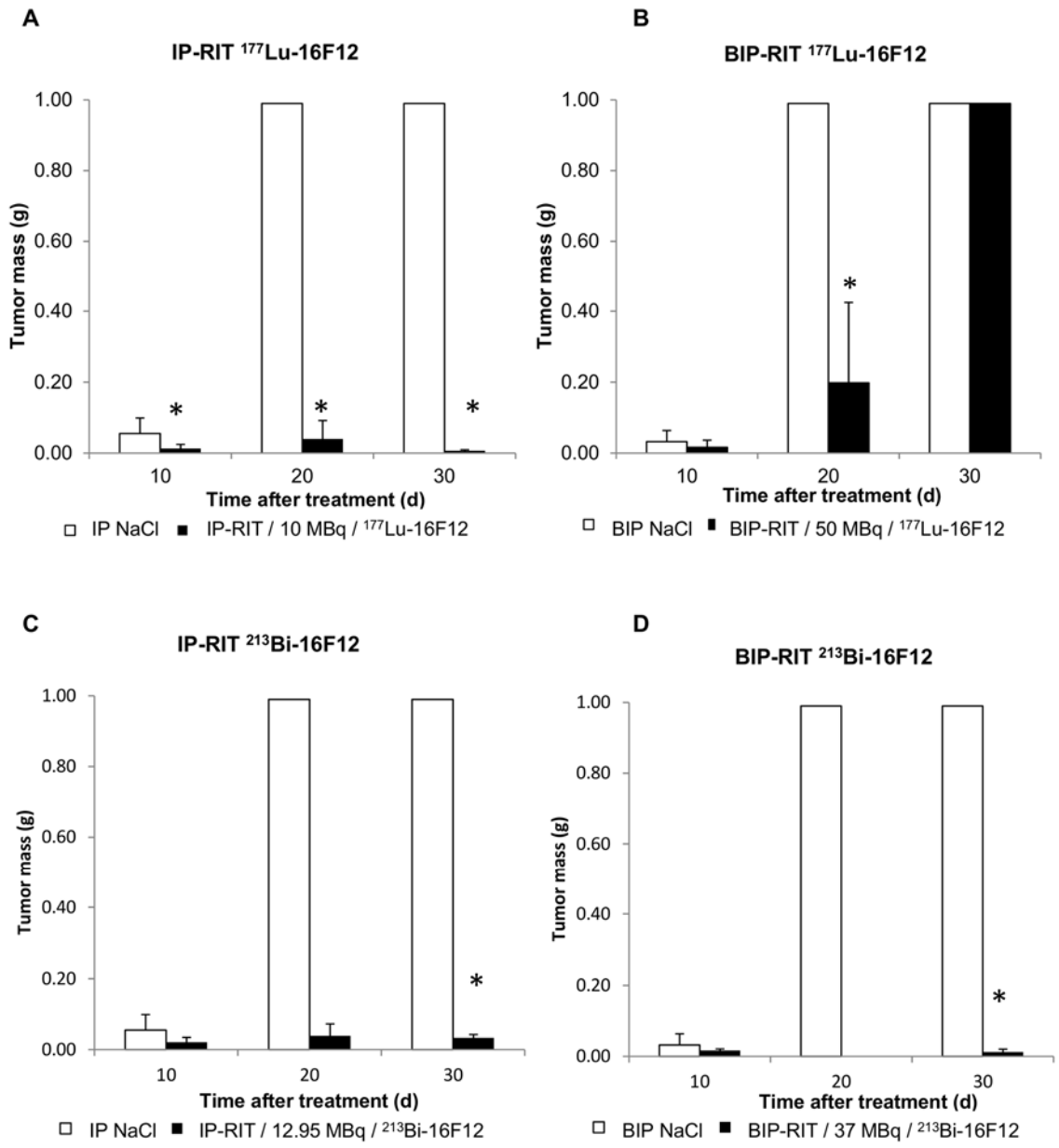

FIGURE 2. Therapeutic efficacy of ^{177}Lu-16F12 (A,B) and ^{213}Bi-16F12 (C,D) after IP-RIT (A, C) and BIP-IP (B, D). Tumor mass (mean ±SD) was calculated at day 10, 20 and 30 after treatment. * $p<0.05$ between therapeutic group (black bars) and NaCl controls (white bars). ¤ $p<0.05$ between ^{213}Bi-16F12 and ^{177}Lu-16F12. + $p<0.05$ between administration routes (IP-RIT versus BIP-RIT; n=7 mice/group).

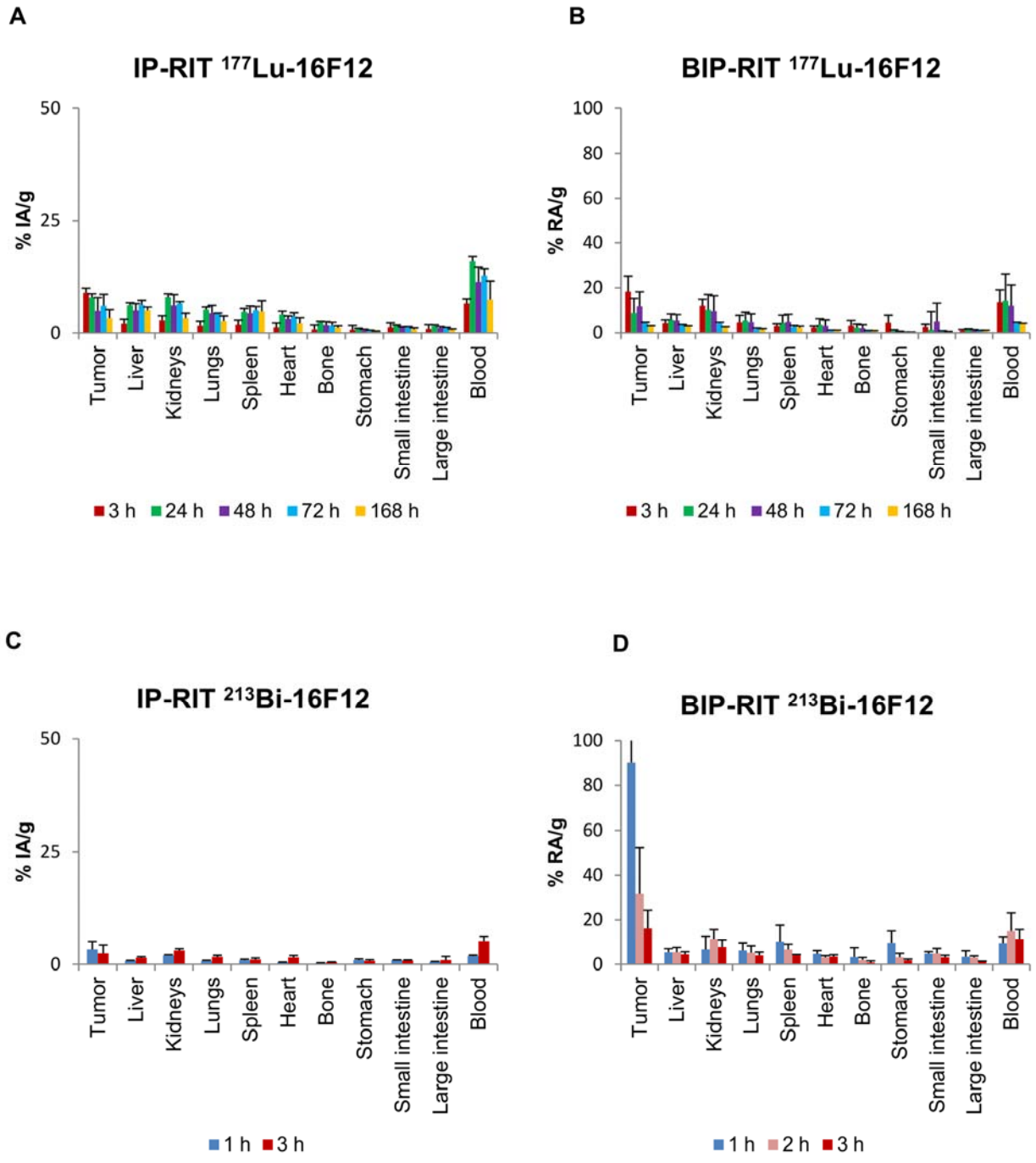

FIGURE 3. Tissue distribution of ^{177}Lu-16F12 (A, B) and ^{213}Bi-16F12 (C, D). Results are given as the mean ± standard deviation of the percentage of injected activity per gram of tissue (%IA/g) after IP-RIT (A, C), and of the percentage of the remaining activity per gram of tissue (%RA/g) after BIP-RIT (B, D) (n=4 mice/group).

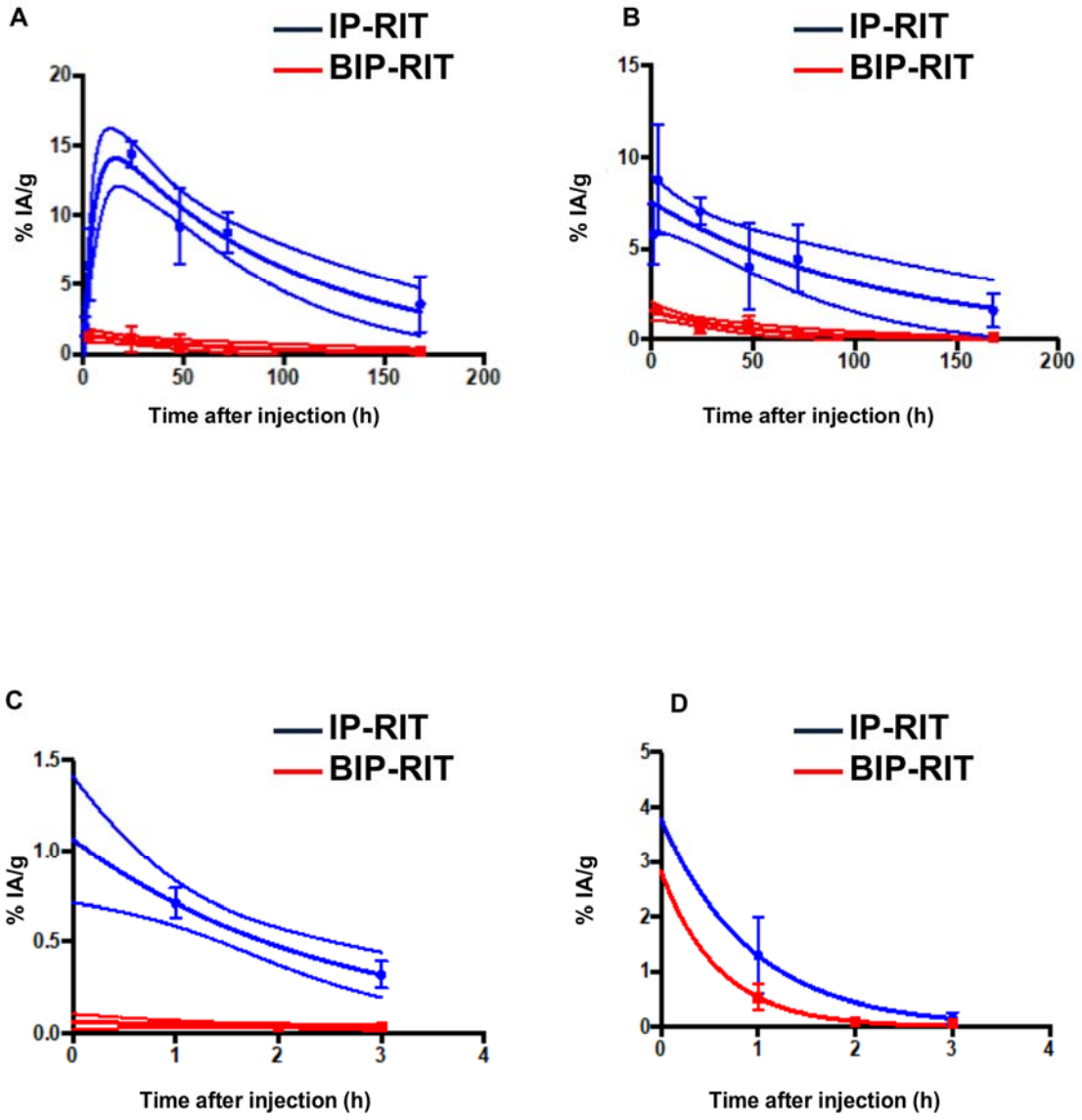

FIGURE 4.

Time activity curves (not corrected for decay) for blood (A) and AN3CA endometrial carcinoma cell tumor xenografts (B) measured with ^{177}Lu-16F12, and for blood (C) and tumor (D) with ^{213}Bi-16F12. Fitting of distribution (with 95% confidence intervals) using mono- or two-exponential components is also shown. This confidence interval was not shown on the tumor graph (D) for sake of clarity.

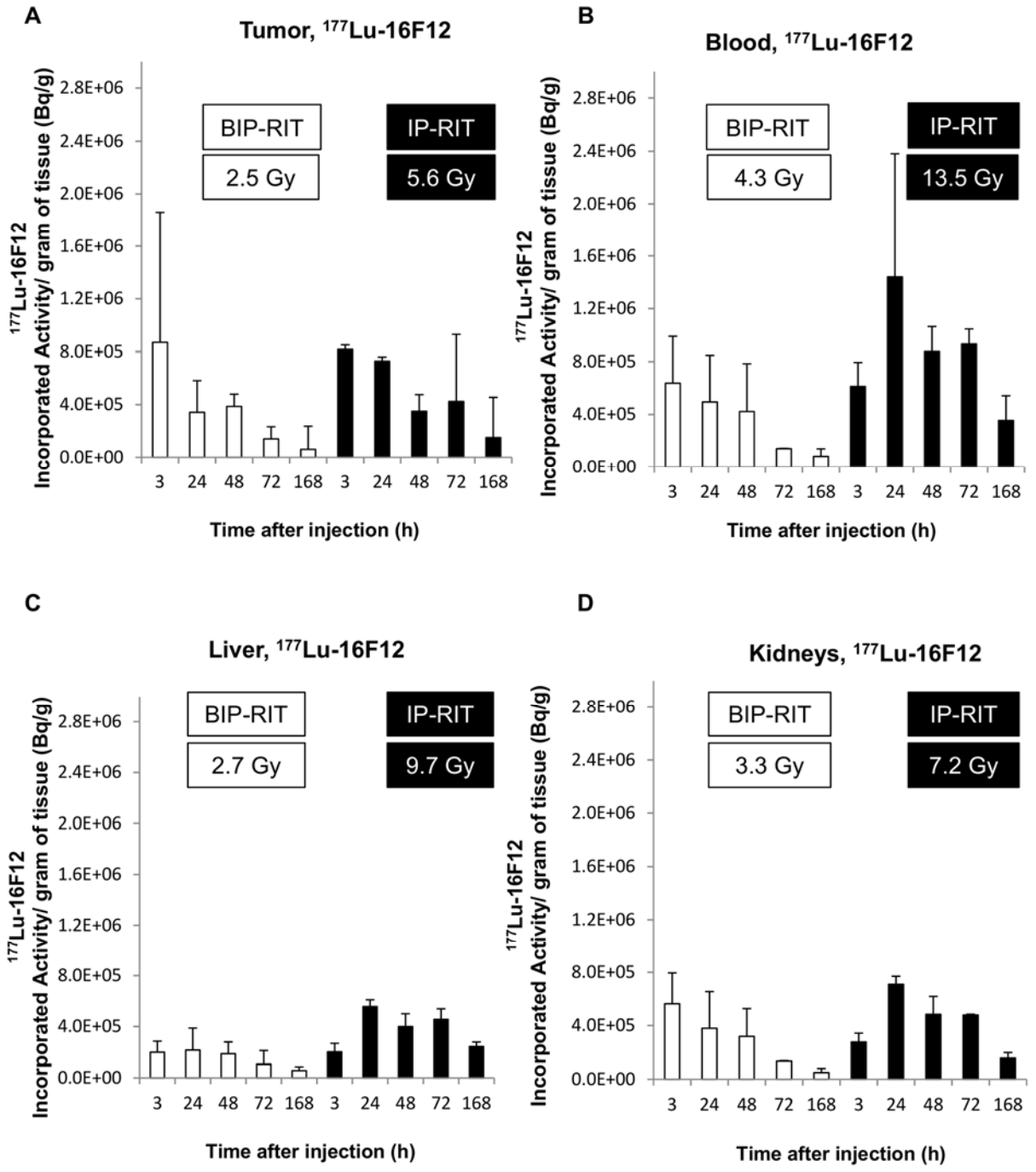

FIGURE 5: Incorporated therapeutic ^{177}Lu-16F12 activity per gram of tissue (Bq/g) over time. Results are shown for tumors (A), blood (B), liver (C) and kidneys (D) after IP-RIT (black bars) or BIP-RIT (white bars). The mean absorbed doses in Gy are also shown.

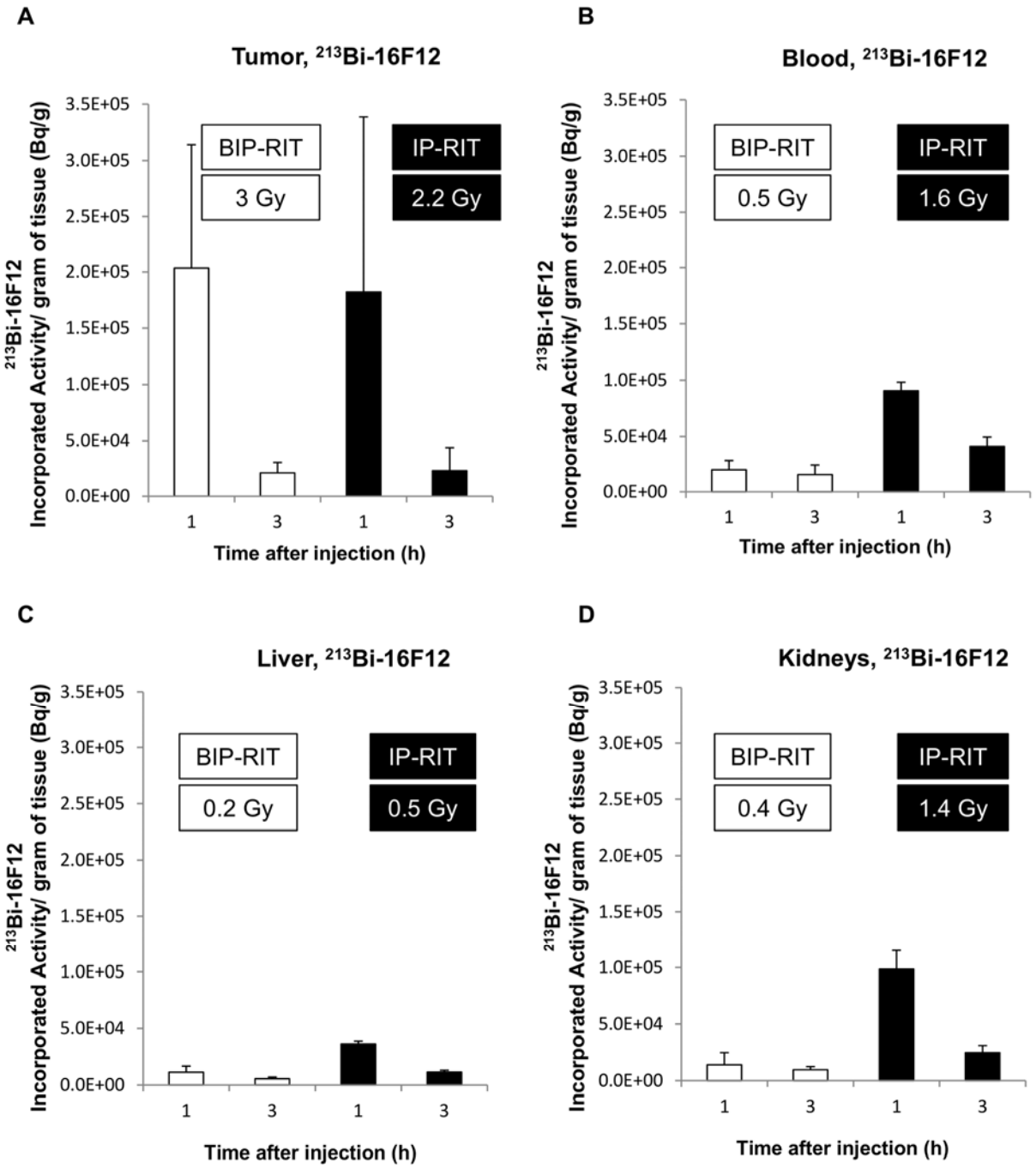

FIGURE 6. Incorporated therapeutic ^{213}Bi-16F12 activity per gram of tissue (Bq/g) over time. Results are shown for tumors (A), blood (B), liver (C) and kidneys (D) after IP-RIT (black bars) or BIP-RIT (white bars). The mean absorbed doses in Gy are also shown.

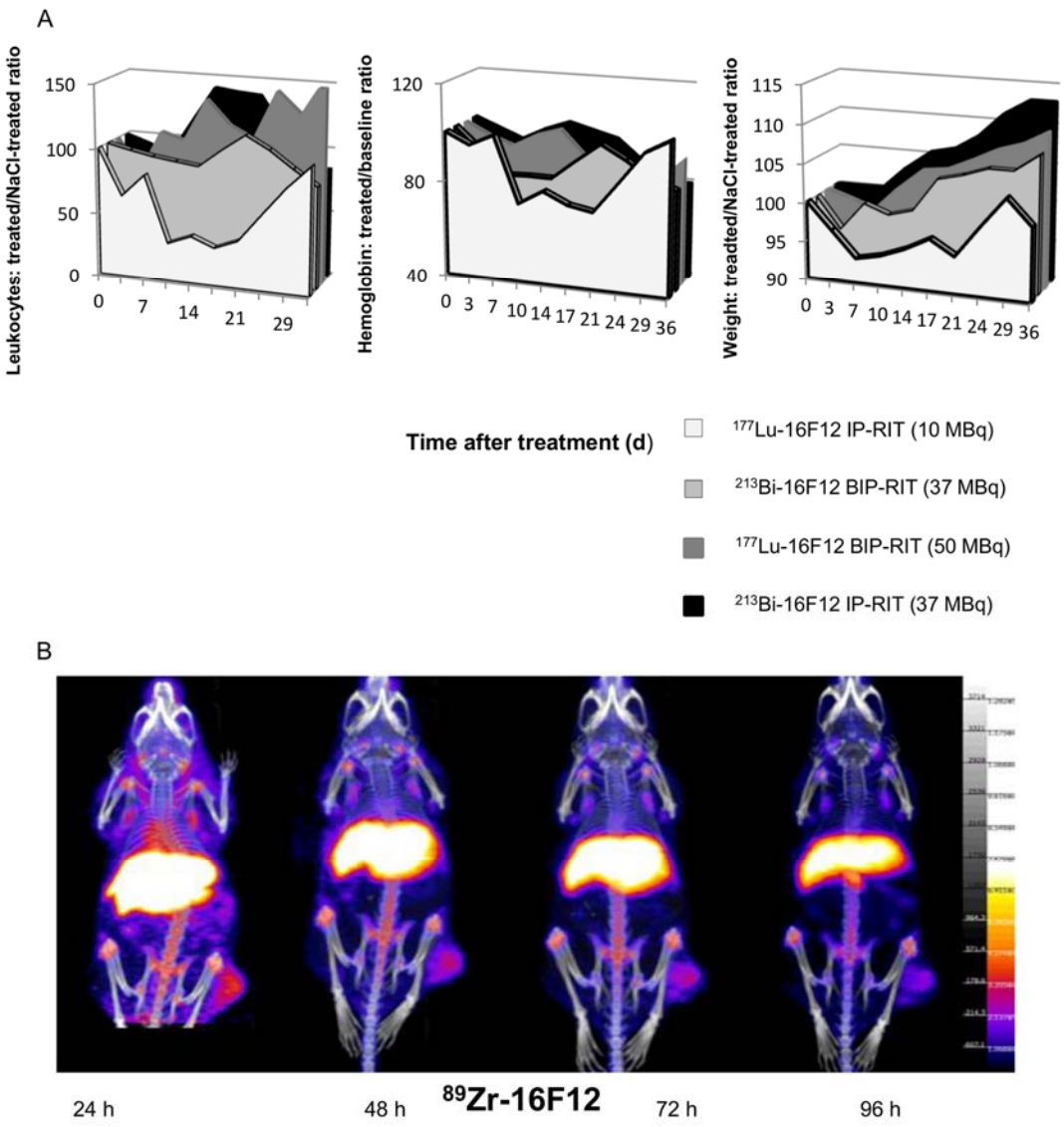

FIGURE 7. Hematological toxicity. White blood cell number (A), hemoglobin level (B) and weight (C) were monitored in healthy mice at various times (day 0 to day 36) after IP-RIT and BIP-RIT with ^{177}Lu-16F12 or ^{213}Bi-16F12, and expressed as the ratio of the value in treated mice relative to control mice (NaCl). Whole-body PET/CT images of mice bearing subcutaneous AN3CA cell tumor xenografts in the right flank at 24, 48, 72 and 96 hours after injection of ^{89}Zr-16F12 (D).

Table 1: Mean absorbed doses following IP-RIT or BIP-RIT with ^{177}Lu-16F12.

	IP-RIT				BIP-RIT			
Tumor/Organ	**Absorbed dose (Gy/MBq)**	**SD**	**Absorbed dose (Gy) Therapy**	**SD**	**Absorbed dose (Gy/MBq)**	**SD**	**Absorbed dose (Gy) Therapy**	**SD**
Blood	1.347	0.305	13.5	3.0	0.086	0.042	4.3	2.1
Tumor	0.560	0.190	5.6	2.1	0.050	0.016	2.5	1.0
Liver	0.973	0.244	9.7	2.4	0.054	0.030	2.7	1.5
Kidneys	0.717	0.171	7.2	1.7	0.066	0.027	3.3	1.3
Lungs	0.461	0.158	4.6	1.6	0.031	0.021	1.5	1.1
Spleen	0.899	0.359	9.0	3.6	0.045	0.031	2.2	1.5
Heart	0.388	0.108	3.9	1.1	0.024	0.018	1.2	0.9
Bones	0.183	0.063	1.8	0.6	0.014	0.008	0.7	0.4
Stomach	0.170	0.021	1.7	0.2	0.011	0.004	0.6	0.2
S. intestine	0.178	0.045	1.8	0.4	0.008	0.003	0.4	0.1
L. intestine	0.056	0.015	0.6	0.1	0.004	0.003	0.2	0.1
Carcass	0.248	0.094	2.5	0.9	0.016	0.007	0.8	0.3
B. marrow	0.456	0.122	4.6	1.2	0.029	0.017	1.5	0.8

Table 2: Absorbed doses calculation following IP-RIT or BIP-RIT with ^{213}Bi-16F12

	IP-RIT				BIP-RIT			
Tumor/Organ	**Absorbed dose (Gy/MBq)**	**SD**	**Absorbed dose (Gy) Therapy**	**SD**	**Absorbed dose (Gy/MBq)**	**SD**	**Absorbed dose (Gy) Therapy**	**SD**
Blood	0.126	0.029	1.63	0.37	0.013	0.010	0.49	0.37
Tumor	0.169	0.227	2.18	2.95	0.081	0.081	3.00	2.98
Liver	0.042	0.011	0.55	0.15	0.004	0.003	0.17	0.10
Kidneys	0.106	0.015	1.37	0.20	0.010	0.013	0.38	0.47
Lungs	0.043	0.017	0.55	0.22	0.004	0.002	0.16	0.09
Spleen	0.046	0.023	0.60	0.30	0.008	0.010	0.30	0.36
Heart	0.038	0.019	0.49	0.25	0.003	0.002	0.12	0.07
Bones	0.013	0.008	0.17	0.10	0.002	0.003	0.08	0.10
Stomach	0.047	0.029	0.61	0.37	0.006	0.007	0.24	0.24
S. intestine	0.045	0.009	0.59	0.11	0.004	0.003	0.15	0.10
L. intestine	0.028	0.015	0.37	0.19	0.003	0.003	0.10	0.11
Carcass	0.033	0.031	0.42	0.40	0.005	0.009	0.20	0.33
B. marrow	0.050	0.012	0.65	0.15	0.005	0.004	0.20	0.15